Analysis of the far infrared H_2–He spectrum

E. Richard Cohen

Science Center, Rockwell International, Thousand Oaks, California 91360

Lothar Frommhold[a] and George Birnbaum

National Bureau of Standards, Washington, D.C. 20234

(Received 6 July 1982; accepted 16 July 1982)

Previous measurements of the far infrared absorption due to H_2–He collisions at the temperatures of 77, 195, and 292 K are analyzed. The spectra are fitted by a semiempirical line shape representing the isotropic induced overlap component and combined anisotropic quadrupolar and overlap components. The experimental spectral moments are evaluated and compared with theory for several induced-dipole and potential models. From the isotropic contribution, the range and strength of the induced dipole is evaluated and compared with the results of *ab initio* calculations. Fitting parameters are obtained with physically plausible temperature dependences which allow simple and accurate representation of the spectra and of their moments at temperatures different from those of the measurements.

I. INTRODUCTION

Interpreting the thermal emission from the major planets requires knowledge of the pressure induced absorption due to H_2–He and H_2–H_2 collisions in the far infrared region.[1] Extensive laboratory studies of the absorption in H_2 have been recently undertaken at a number of temperatures from 77 to 300 K and over a range of frequencies extending from about 30 cm^{-1} to nearly 2000 cm^{-1}.[2–4] In order to apply these results to planetary atmospheres, one must be able to compute the absorption at a variety of temperatures and pressures different from those at which the measurements were made. A semiempirical line shape[3–6] has been developed which is useful for this purpose, since it accurately represents the spectra over a wide temperature range.

Because of the relative simplicity of the spectrum, namely a few relatively well resolved lines, the study of the far infrared absorption in H_2 and H_2–He is also important for elucidating the nature of collision-induced translation-rotation spectra and the molecular interactions involved. In this work, we use the above semiempirical line shape to analyze the H_2–He spectra measured previously at 77.4, 195, and 292 K. The spectra are represented in terms of two collision-induced components, one due to an isotropic overlap dipole and the other to an anisotropic dipole consisting of a quadrupole and an overlap induced part. The spectral moments evaluated from those components are compared with theory for several induced dipole and potential functions. Satisfactory agreement at all temperatures is obtained for the prominent isotropic component with an *ab initio* induced dipole and a recent empirical potential based on a beam scattering measurement (Table II).

II. THEORY

The absorption coefficient, $\alpha(\omega)$ (cm^{-1}), due to the dipoles induced in binary encounters between unlike particles a and b, is described by[5,6]

$$\alpha(\omega)=\frac{4\pi^2 n_a n_b}{3\hbar c}\,\omega[1-\exp(-\beta\hbar\omega)]\sum_{L\lambda}\sum_{JJ'}\rho_J(2J+1)\times C(J\lambda J';00)^2 S_{L\lambda}\Gamma_{L\lambda}(\omega-\omega_{JJ'})\ . \tag{1}$$

Here n_a and n_b are number densities of the components a and b, $\beta=1/kT$, J is the angular momentum quantum number, and $\omega_{JJ'}=2\pi c(\nu_{J'}-\nu_J)$ is the angular transition frequency. The rotational energy levels of hydrogen (in wave numbers) are given by[7]

$$\nu_J=59.3392\,J(J+1)-0.045\,99J^2(J+1)^2+0.000\,052\,J^3(J+1)^3\ \text{cm}^{-1}\ . \tag{2}$$

The Boltzmann factor ρ_J is

$$\rho_J=g_J\,e^{-\beta E_J}\Big/\sum_{J'}(2J'+1)\,g_{J'}\,e^{-\beta E_{J'}}\ , \tag{3}$$

where $E_J=hc\nu_J$ is the energy of rotational state J. The statistical factors due to nuclear spin are $g_J=1$ for even J and $g_J=3$ for odd J.

The line shape functions are the Fourier transforms of the reduced correlation functions,[5] and $S_{L\lambda}$ is an intensity factor. It is related to expansion coefficients $A_{L\lambda}(R)$ of the induced dipole moment[8,14] with angular dependence L,λ by

$$S_{L\lambda}=\langle A^2_{L\lambda}(R)\rangle\ , \tag{4}$$

where $\langle\cdots\rangle$ signifies a thermal average [see Eq. (A1)]. These coefficients, which are defined in the Appendix, have the dimensions of dipole moment and are functions of internuclear separation R. Only three A coefficients need to be considered here, namely the isotropic overlap-induced component labeled $L,\lambda=1,0$, the anisotropic pure overlap component ($L,\lambda=1,2$), and the anisotropic mixed overlap and quadrupole-induced component ($L,\lambda=3,2$). There is, furthermore, a small hexadecapole induced dipole A_{54}, which will be ignored. To simplify the notation, we use the subscript i for isotropic (instead of $L,\lambda=1,0$), as in $S_i=S_{10}$. We assume that the anisotropic components may be represented by a single shape function

[a]On leave from the Physics Department, The University of Texas at Austin, Austin, TX 78712.

$$S_q\Gamma_q(\omega-\omega_{JJ'})\cong S_{12}\Gamma_{12}(\omega-\omega_{JJ'})+S_{32}\Gamma_{32}(\omega-\omega_{JJ'}) , \quad (5)$$

where $S_{12}+S_{32}=S_q$. This approximation is necessary because the available data are not of sufficient precision to allow a separation into two anisotropic parts. In the semiempirical line shape analysis presented here, the component $S_{32}\Gamma_{32}(\omega-\omega_{JJ'})$ may be regarded as a composite term represented by the sum of three components arising from the quadrupole and overlap induced dipoles and their interference. The sum over L,λ in Eq. (1) becomes

$$\sum_{L\lambda}\sum_{JJ'}\rho_J(2J+1)C(J\lambda J';00)^2S_{L\lambda}\Gamma_{L\lambda}(\omega-\omega_{JJ'})$$
$$=S_i\Gamma_i(\omega)+\sum_{JJ'}\rho_J(2J+1)C(J2J';00)^2S_q\Gamma_q(\omega-\omega_{JJ'}) . \quad (6)$$

The shape function is modeled by[5,6]

$$\Gamma(\omega)=\frac{\tau_1}{\pi}\left[\exp\left(\frac{\tau_2}{\tau_1}+\tau_0\omega_-\right)\right]\frac{zK_1(z)}{1+\omega_-^2\tau_1^2} , \quad (7)$$

with

$$z=\frac{\tau_3}{\tau_1}[1+(\omega_-\tau_1)^2]^{1/2} ;\quad \tau_3^2=\tau_2^2+\tau_0^2 ;\quad \tau_0=\beta\hbar/2 ;$$
$$\omega_-=\omega-\omega_{JJ'} .$$

The quantities Γ, S, τ_1, and τ_2 will be subscripted with the letter q or i to distinguish the quadrupole plus anisotropic overlap-induced components (q) and the isotropic component (i), which have different shapes. The function $\Gamma(\omega)$ is normalized so that its zeroth moment equals unity $\int\Gamma(\omega)\,d\omega=1$. The strength parameter S thus becomes the zeroth moment of each component. Similarly, the first moment is related to the product $\tau_1\tau_2$, according to

$$\int_{-\infty}^{\infty}\omega\,\Gamma(\omega)\,d\omega=\tau_0/\tau_1\tau_2 . \quad (8)$$

$K_1(z)$ is the modified Bessel function of the second kind with the properties

$$zK_1(z)\to 1 \text{ for } z\to 0 ;\quad K_1(z)\to\sqrt{(\pi/2z)}\,e^{-z} \text{ for } z\gg 1 . \quad (9)$$

The time parameter τ_2 controls the exponential decay of the wings. When $\tau_1\gg\tau_2$ the shape is Lorentzian in the vicinity of the transition frequency, with a half-width given approximately by $\Delta\omega_1=\tau_1^{-1}$. However, when $\tau_2/\tau_1\sim 1$, as is true for H_2, Eq. (8) is never accurately Lorentzian and $\Delta\omega_1$ differs appreciably from the half-width that would be obtained by attempting to fit data to a Lorentzian, as has been done in the past (see, e.g., Ref. 9).

The Clebsch–Gordan coefficients $C(J2J';00)$ vanish for $|J-J'|>2$. Their symmetry allows us to write

$$\sum_{JJ'}\rho_J(2J+1)C(J2J';00)^2\Gamma_q(\omega-\omega_{JJ'})$$
$$=A\Gamma_q(\omega)+\rho_0\Gamma_q(\omega-\omega_{02})+\rho_2\Gamma_q(\omega+\omega_{02})$$
$$+\tfrac{9}{5}[\rho_1\Gamma_q(\omega-\omega_{13})+\rho_3\Gamma_q(\omega+\omega_{13})]$$
$$+\tfrac{18}{7}[\rho_2\Gamma_q(\omega-\omega_{24})+\rho_4\Gamma_q(\omega+\omega_{24})]$$
$$+\tfrac{10}{3}[\rho_3\Gamma_q(\omega-\omega_{35})+\rho_5\Gamma_q(\omega+\omega_{35})]+\cdots , \quad (10)$$

with the same function $\Gamma_q(\omega)$ throughout, but shifted by the rotational frequencies which may be positive or negative (up or down transition). Here we have set

$$A=\sum_J\rho_J(2J+1)/J(J+1)/(2J-1)(2J+3) . \quad (11)$$

In Eq. (10), the first term represents a small contribution to the translational band ($\omega_{JJ}=0$) while the other terms are related to collision-induced transitions to a higher or lower rotational level.

In summary, we see that Eq. (1) with Eqs. (7) and (10) can be fitted with six parameters: τ_{1q}, τ_{2q}, and S_q associated with the quadrupole and anisotropic overlap-induced dipoles, and τ_{1i}, τ_{2i}, and S_i associated with the isotropic overlap-induced dipole. The actual situation is more complex, but the present data do not have sufficient precision and do not extend to high enough frequencies to allow the quadrupolar and anisotropic overlap components to be resolved into separate contributions.

III. ANALYSIS OF THE SPECTRA

Figures 1 to 3 show the experimental spectra (dots) of Ref. 2. At the highest temperature the $S_0(1)$ line structure is prominent. The strong translational spectrum is superimposed with the relatively weak, unresolved $S_0(0)$ line. At the lowest temperature, on the other hand, the translational, $S_0(0)$ and $S_0(1)$ line structures are quite well resolved. Before a fit of these spectra can be attempted, a suitable measure of the quality of the fit must be defined. Since the measurements were taken in such a way that the *relative* uncertainty remains about the same for all intensity readings, we will attempt a fit by minimizing the sum of squares of relative deviations, namely

$$\Delta^2=\sum_{i=j}^{148}\{[\alpha_i-\alpha(\omega_i)]/\alpha(\omega_i)\}^2 . \quad (12)$$

Here, α_i is the measured absorption coefficient at the frequency ω_i, and $\alpha(\omega)$ is the six-parameter model line shape. It is sufficient to account for the five lowest rotational transitions ($J=0$ to 4, $\Delta J=2$). We mention that each spectrum comprises 148 data points, but at the two higher temperatures the first few points were suppressed ($j=5$ at 292 K; $j=7$ at 195 K; $j=1$ at 77 K) on account of the sharp falloff to zero frequency, which may in part be related to intercollisional interference. The Bessel function $K_1(z)$ is approximated[10] to better than 2.2×10^{-7}. The nonlinear least-mean squares routine is of the Levenberg–Marquardt type.[11] The residual rms deviation of the fit is defined according to

$$\epsilon=\sqrt{\Delta^2/(143-j)}\times100\% , \quad (13)$$

which gives the average residual relative deviation.

We note that *at the temperature of* 195 K the least-mean squares method converges rapidly to the solution shown in Table I (marked unconstrained fit) for any startup vector which did not lead to divergence. The rms deviation amounts to $\epsilon\cong4\%$, which compares favorably with the experimental uncertainty (at least about twice that amount). The uncertainty of the solu-

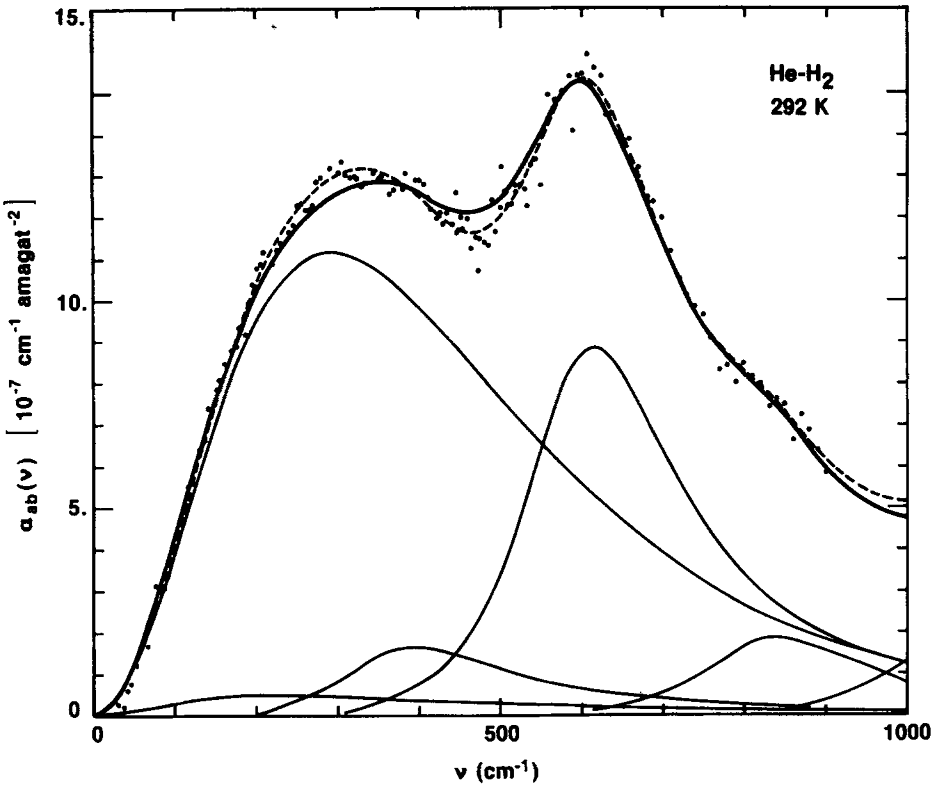

FIG. 1. The fitted CIA spectrum at 292.4 K. Dots: measurement (Ref. 2), heavy line: constrained (preferred) fit of the measurement; dashed: unconstrained (closest) fit. Light lines show the isotropic line, the anisotropic translational, $S_0(0)$, $S_0(1)$, and $S_0(2)$ lines and the low frequency wing of $S_0(3)$ line.

tion, derived from the goodness of the fit, amounts to 1% for S_i, 2% for the product $\tau_{1i}\tau_{1i}$, 3% for S_q, about 5% for τ_{1i}, τ_{2i}, τ_{1q}, and 13% for τ_{2q}. Individual τ_2 values show a greater uncertainty than the products of $\tau_1\tau_2$. These error estimates reflect only the statistical uncertainty of the fitting at 195 K, the best of the three fits. They do not account for systematic errors of the experiment.

At 77 and 292 K, convergence of the least-mean squares routine could be achieved over a wide range of input parameters, but not to a unique solution. Instead, several solutions emerged which varied widely relative to each other. The mean residual error was consistently small at 292 K, $\epsilon \cong 4\%-5\%$ and $\epsilon \simeq 12\%-16\%$ at 77 K. The solutions with the smallest ϵ are listed in Table I ("unconstrained fit"), but several others had only insignificantly higher values for ϵ. Statistical errors for these were nearly twice (at 292 K), and thrice (at 77 K) the values obtained at 195 K.

It must be emphasized that the fittings showed much

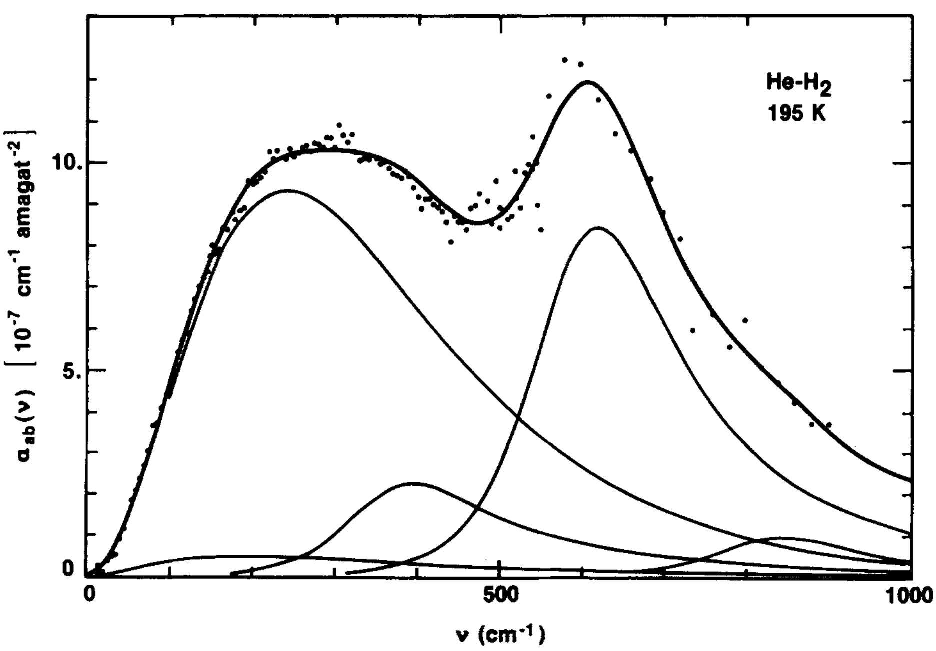

FIG. 2. The fitted CIA spectrum at 195 K. Details are as in Fig. 1, except that the unconstrained fit was virtually identical with the constrained one and is not shown.

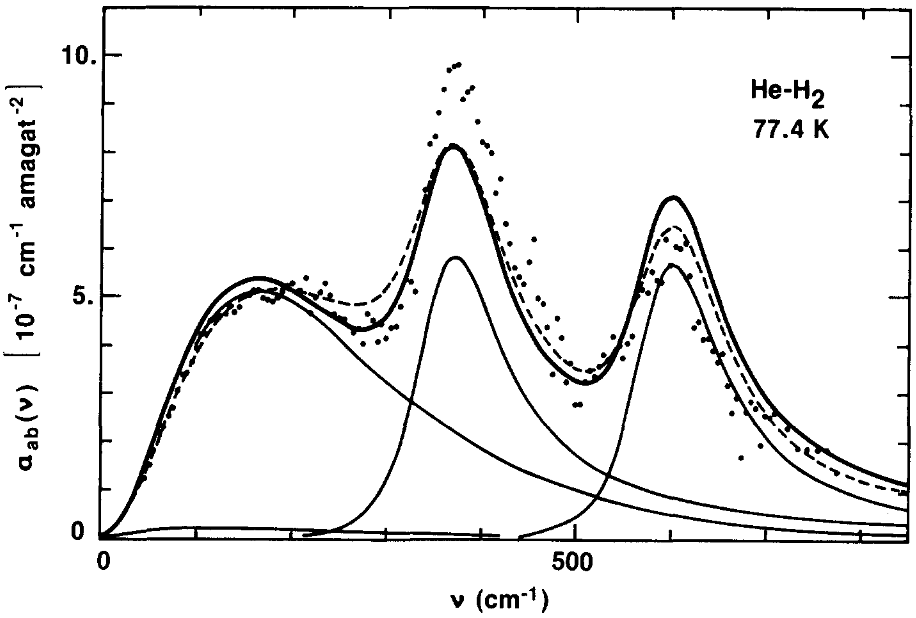

FIG. 3. The fitted CIA spectrum at 77.4 K. Details are as in Fig. 1, except for the $S_0(2)$ and $S_0(3)$ lines which are of negligible intensity and are not shown.

flexibility and that a wide range of parameter sets could approximate the experimental curves with comparable accuracy. Undoubtedly, the inaccuracy in the data contributed to the difficulty in obtaining unique parameter sets at two temperatures. The adjustment is statistically loose and the least squares fittings show strong correlations. To a certain extent, one can adjust for changes in one parameter by making compensating changes in the others.

The unconstrained fits thus obtained are shown in Figs. 1 to 3 (dashed curves) along with the measurements. Also shown are the isotropic translational and the weak translational anisotropic components, along with the various rotational lines. We note that the translational band intensity of the isotropic overlap component is much greater than that of the quadrupolar component. Comparison with the induced spectra in pure hydrogen shows that the $S_0(0)$ and $S_0(1)$ lines of H_2-He have much less intensity. This results from the smaller polarizability of He compared with H_2, which substantially reduces the quadrupole-induced dipole component.

It appears that the discrepancies between the fitted and measured spectra for H_2-He may be attributed to the inaccuracy of the experimental results. Whereas the translational spectrum at low frequencies ($< \omega_{12}$) can be determined with good accuracy, the rotational structure of the spectrum due to H_2-He collisions is less well defined. As explained in Ref. 2, this arises in the case of H_2-He mixtures with too high an H_2 concentration which yields the absorption coefficient due to H_2-He collisions as a small difference between two large numbers. In any case, it was not possible to obtain the rotational line structure of H_2-He with an accuracy as high as for pure H_2.

While the fits discussed above are *per se* quite acceptable, some of the six parameters when plotted as function of temperature (Figs. 4 and 5) do not follow a simple law as they should. According to theory (dashed lines in Figs. 4 and 5), S is expected to vary approxi-

TABLE I. The fits of the H_2-He spectrum.[a]

	S_i $K\,Å^6$	τ_{1i} 10^{-14} s	τ_{2i} 10^{-14} s	S_q $K\,Å^6$	τ_{1q} 10^{-14} s	τ_{2q} 10^{-14} s	ϵ %
292.4 K							
Reference 6	119.1	1.91	2.52	21.0	4.20	2.86	6.1
unconstrained fit	108.7	1.14	6.12	36.6	4.23	1.55	4.2
constrained fit	119.9	1.90	3.05	27.5	4.36	1.93	4.7
195 K							
Reference 6	81.3	1.99	4.22	19.1	4.13	2.38	5.6
unconstrained fit	82.4	2.10	4.30	21.8	4.51	2.43	3.9
constrained fit	83.3	2.16	4.19	21.7	4.57	2.40	4.0
77.4 K							
Reference 6	34.5	3.64	4.66	6.93	7.02	13.44	21.4
unconstrained fit	35.8	3.91	3.95	7.77	8.16	8.99	12.7
constrained fit	33.5	3.43	6.56	12.06	9.36	2.88	15.5

[a]Measurements from Ref. 2.

mately as T^m. The product $\tau_1\tau_2$ should be approximately inversely proportional[5] to T. It is reasonable to expect that the individual τ_1, τ_2 should be approximately proportional to $T^{-1/2}$.

We have, therefore, attempted another fit with the constraint that in a double logarithmic plot linear relationships are approximated as much as possible. *Any* linear relationship was deemed acceptable. This worked well particularly for the isotropic part, with fits featuring residual rms deviations only slightly greater than for the unconstrained fits (Table I). The straight lines obtained for the strength parameters S, and for the product $\tau_1\tau_2$ approximated very closely an exact direct, and an inverse temperature dependence, respectively, given by

$$S_i = 33.53\ \mathrm{K\,Å^6}(T/77.4\ \mathrm{K})\ , \tag{14}$$

$$\tau_{1i}\tau_{2i} = 22.5\times10^{-28}\ \mathrm{s^2}(77.4\ \mathrm{K}/T)\ , \tag{15}$$

$$\tau_{1i} = 3.43\times10^{-14}\ \mathrm{s}\,(77.4\ \mathrm{K}/T)^{1/2}\ , \tag{16}$$

with an analogous equation for τ_{2i} given by the ratio of Eqs. (15) and (16). Similarly, for the anisotropic part, we obtain with reasonable precision (Fig. 5)

$$S_q = 12.06\ \mathrm{K\,Å^6}\ (T/77.4\ \mathrm{K})^{0.57}\ , \tag{17}$$

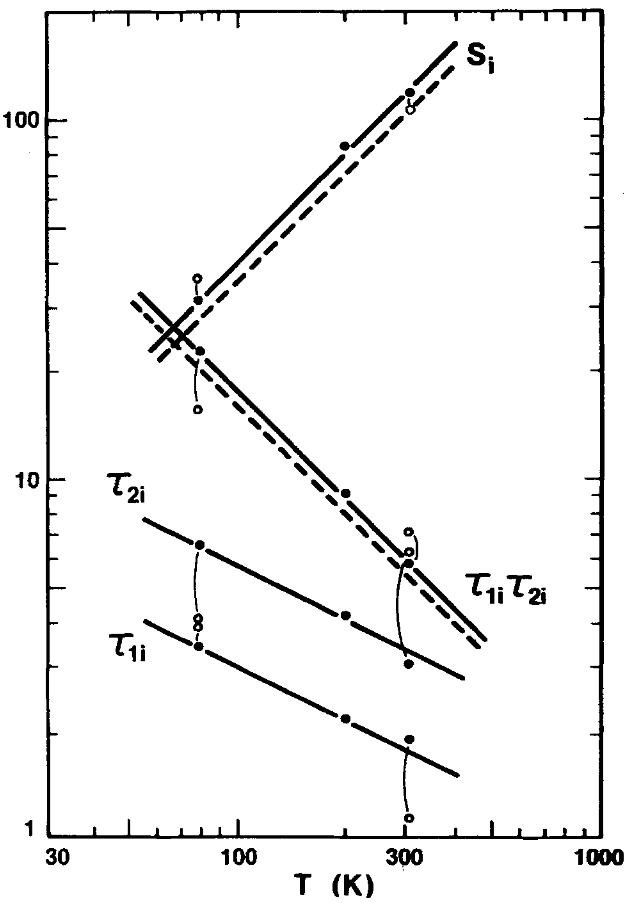

FIG. 4. Isotropic parameters of the fit: τ_{1i}, τ_{2i}, (10^{-14} s); S, (K Å^6). Full circles: constrained (preferred) fit; open circles; unconstrained fit (if different from the former). Heavy lines: Eqs. (14–16); dashed lines: from theoretical prediction based on Wormer and van Dijk's induced dipole (Ref. 16), on the empirical beam scattering potential (Ref. 17), and on Eqs. (25, 26), where α_{1i} and γ_{1i} are given in the Appendix.

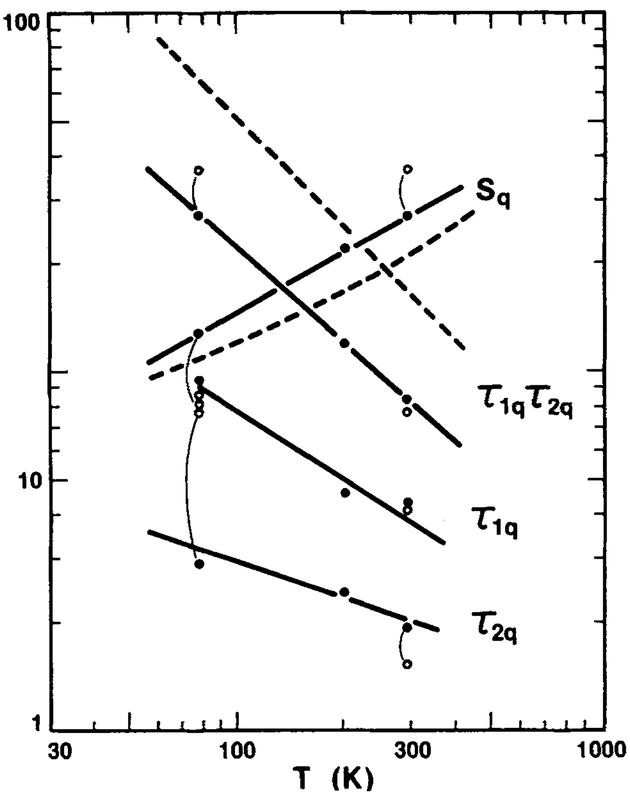

FIG. 5. Anisotropic parameters of the fit: details as in Fig. 4, but using Eqs. (17)–(19) and Eqs. (23), (24), where α_{1q} and γ_{1q} are defined in the Appendix of Ref. 4.

$$\tau_{1q}\tau_{2q} = 27.0\times10^{-28}\ \mathrm{s^2}\ (T/77.4\ \mathrm{K})^{-0.90}\ , \tag{18}$$

$$\tau_{2q} = 3.02\times10^{-14}\ \mathrm{s}\,(T/77.4\ \mathrm{K})^{-0.30}\ , \tag{19}$$

with an equation for τ_{1q} given by the ratio of Eqs. (18) and (19). On physical grounds, the constrained fits are expected to approximate reality more closely than the unconstrained ones. They are only insignificantly inferior as the last column of Table I shows, and are in reasonable agreement with theory (dashed lines, Figs. 4 and 5, to be discussed with Table II below).

As may be expected from our previous discussion, the constrained solution vector at 195 K barely differs from the unconstrained one. Apparently, this measurement is the most accurate, and the most discriminating of the three.[26] To a certain extent, this fact can be understood from the circumstances of the experiment,[2] namely a stable temperature and an optical transmission of the system less subject to drift than at the other temperatures. Also, since n-H_2 and e-H_2 are not too different, the measurements were not as dependent on the efficiency of the *ortho-para* equilibrium as at 77 K.

Before leaving the discussion of the fitting procedures, we note that if one plots the spectral density as in Ref. 6,

$$D(\nu) = \alpha(\nu)/[\rho^2\nu\tanh(\beta h\nu c/2)]\ , \tag{20}$$

there is a rapid decrease in $D(\nu)$ at low frequencies at 195 and 292 K which might be attributed to the intercollisional interference effect.[12,13] However, an analysis of the data shows that these dips are probably not statistically significant. It should be noted that dividing

TABLE II. Comparison of theoretical and measured spectral invariants.

	77.4 K	195 K	292.4 K	77.4 K	195 K	292.4 K
Isotropic Component		$\gamma_{1i}/(10^{-58}\ \mathrm{cm}^5\ \mathrm{s})$			$\alpha_{1i}/(10^{-31}\ \mathrm{cm}^5/\mathrm{s})$	
unconstrained fit	1.016	0.927	0.816	0.658	1.024	1.165
constrained fit	0.951	0.938	0.900	0.423	1.034	1.554
theory[a]	0.816	0.792	0.828	0.403	0.971	1.511
Anisotropic Component		$\gamma_{1q}/(10^{-58}\ \mathrm{cm}^5\ \mathrm{s})$			$\alpha_{1q}/(10^{-31}\ \mathrm{cm}^5/\mathrm{s})$	
unconstrained fit	0.220	0.246	0.275	0.330	1.065	1.829
constrained fit	0.342	0.245	0.206	0.592	1.059	1.305
theory[a]	0.309	0.190	0.159	0.477	0.751	0.950
Total		$\gamma_1/(10^{-58}\ \mathrm{cm}^5\ \mathrm{s})$			$\alpha_1/(10^{-31}\ \mathrm{cm}^5/\mathrm{s})$	
unconstrained fit	1.236	1.173	1.091	0.988	2.089	2.994
constrained fit	1.293	1.183	1.106	1.015	2.093	2.859
theory[a]	1.125	0.982	0.987	0.880	1.722	2.461

[a]Theory based on *ab initio* induced dipole of Wormer and van Dijk (Ref. 16) and the empirical potential of Gengenbach and Hahn (Ref. 17).

$a(\nu)$ by ν^2 at low frequencies to obtain $D(\nu)$ greatly amplifies any errors in the low frequency data. Moreover, our attempt to fit the dip by an inverted Lorentz shape according to the theory of the intercollisional interference effect was unsatisfactory. A Lorentz width was obtained which appeared to be too large by a factor of 2 on the basis of a comparison with the dip seen in the Q branch of the fundamental band.[8] For these reasons, we eliminated the first four points (at 292 K) and six points (at 195 K) from the data for our fitting procedure.

IV. SPECTRAL MOMENT ANALYSIS

The spectral invariants α_1 and γ_1 are defined by

$$\alpha_1 = \alpha_{1i} + \alpha_{1q} = [n_a n_b]^{-1} \int_0^\infty \alpha(\omega)\, d\omega \ , \tag{21}$$

$$\gamma_1 = \gamma_{1i} + \gamma_{1q} = \frac{1}{n_a n_b} \int_0^\infty \frac{\tau_0 \alpha(\omega) d\omega}{\omega \tanh(\omega\tau_0)} \ . \tag{22}$$

The isotropic and anisotropic components may be obtained from the parameters of the fitted spectrum. Thus, following the derivation of Eqs. (31b) and (35) in Ref. 5 we write

$$\alpha_{1q} = \gamma_{1q} \left(\frac{6kT}{I} + \frac{1}{\tau_{1q}\tau_{2q}} \right) \ , \tag{23}$$

$$\gamma_{1q} = \frac{2\pi^2}{3kTc} S_q \ , \tag{24}$$

for the anisotropic contribution. Here, I is the moment of inertia of H_2 defined by the rotational constant $B_0 = \hbar/4\pi c I$ (cm^{-1}). The quantity $\gamma_{1q}(6kT/I)$ describes that part of α_{1q} which results from the rotational transitions $\Delta J = \pm 2$, while $\gamma_1/\tau_{1q}\tau_{2q} = \alpha_{1t}$ is the translational contribution $\Delta J = 0$ plus the contributions arising from the translational broadening of the rotational lines. The isotropic overlap contribution can be expressed similarly as

$$\alpha_{1i} = \gamma_{1i}/\tau_{1i}\tau_{2i} \ , \tag{25}$$

$$\gamma_{1i} = \frac{2\pi^2}{3kTc} S_i \ . \tag{26}$$

Theoretical expressions for the moments α_1, γ_1 are given in the Appendix.

While measured isotropic and anisotropic components [Eqs. (23)–(26)] show substantial variation between constrained and unconstrained fits except at 195 K, their sum is nearly independent of the fitting procedure as expected, with an accuracy of a few percent (Table II). The observed flexibility of the fits at 77 and 292 K is related to intensities which are shifted back and forth between the isotropic and anisotropic components. Individual parts are, therefore, not well known except at 195 K where the separation was for a variety of reasons well defined. The constrained fit apparently is the best approximation we have available of a realistic separation of the measurements into isotropic and anisotropic parts.

The invariants α_{1i}, γ_{1i}, α_{1q}, and γ_{1q} can be computed from theory (Table II) with the relationships discussed in the Appendix if the interaction potential and the induced dipole, resolved into its proper symmetry components,[14–16] are known. Various interaction potentials have been obtained for the H_2–He systems; only the isotropic part of the potential is considered. Of these, we mention the empirical model by Gengenbach and Hahn[17] based on accurate beam scattering data at energies from 0.000 14 to 2.9 eV. Such a range defines the region of repulsive interaction near the root σ, which is so important for collision-induced absorption. Furthermore, we consider the *ab initio* potentials by Meyer *et al.*[18] and by Mulder *et al.*[19] which, for our purpose are nearly identical. For historical reasons moments based on the Lennard-Jones (LJ) 6–12 model used in earlier work on the subject[20] are also given.

We use the induced dipole model of Wormer and van Dijk,[16] supplemented by the isotropic dispersion coefficient of Berns *et al.*,[15] and the empirical interaction potential[17] to compute the theoretical moments

TABLE III. Theoretical moments for different potentials.

Isotropic Component basis		77 K	195 K	295 K	77 K	195 K	295 K
$V(R)$	$\mu(R)$	$\gamma_{1i}/(10^{-58}$ cm^5 s)			$\alpha_{1i}/(10^{-31}$ cm^5/s)		
Ref. 17	Ref. 16	0.816	0.792	0.828	0.403	0.971	1.511
Ref. 18	Ref. 16	0.744	0.691	0.752	0.368	0.850	1.374
Ref. 18	Ref. 15	0.722	0.706	0.797	0.400	0.970	1.629
Ref. 19	Ref. 15	0.716	0.730	0.787	0.396	1.007	1.615
Ref. 20[a]	Ref. 15	1.543	1.166	1.070	0.847	1.583	2.177
Anisotropic Component		$\gamma_{1q}/(10^{-58}$ cm^5 s)			$\alpha_{1q}/(10^{-31}$ cm^5/s)		
Ref. 17	Ref. 16[b]	0.309	0.190	0.159	0.477	0.751	0.950
Ref. 18	Ref. 16[b]	0.302	0.178	0.150	0.466	0.703	0.892
Ref. 18	Ref. 15[c]	0.177	0.094	0.0733	0.262	0.354	0.418
Ref. 19	Ref. 15[c]	0.173	0.094	0.0736	0.257	0.355	0.419
Ref. 20	Ref. 15[c]	0.239	0.119	0.0889	0.358	0.453	0.509

[a]L-J 6-12 potential.
[b]Contains both quadrupole and overlap (Wormer and van Dijk).
[c]Quadrupole component only (Berns, Wormer, Mulder, and van Avoird).

given in Table II. The classical low-density limit of the radial distribution function is used with quantum corrections[21] to order $\hbar^2$. The comparison with the experiment shows that the total theoretical moments α_1, γ_1 are smaller than the measured values by 15%–20%. This agreement is gratifying considering the difficulties of the measurement and the uncertainties of the induced model and, perhaps, the potential. The experimental isotropic γ_{1i} shows about the same deviation from theory, but theoretical and experimental α_{1i} agree to within a surprising $\sim 5\%$.

Figure 4 compares theoretical and experimental values of S and $\tau_1\tau_2$ for the isotropic component. We see from Eq. (26) that the strength parameter S_i is directly related to the invariant γ_{1i}. From Eq. (25) we see that the product $\tau_{1i}\tau_{2i}$ is given by the ratio of α_{1i} and γ_{1i}. Therefore, we can compute S_i and $\tau_{1i}\tau_{2i}$ from theory (dashed lines in Fig. 4). The quantities S_i and $\tau_{1i}\tau_{2i}$ and their temperature dependence determined by measurement are closely approximated by theory. With the help of Eqs. (24) and (25) an analogous computation is possible for the anisotropic component (Fig. 5).

Returning to Table II, we see that the theoretical anisotropic moments are smaller by 20%–40% than their experimental counterparts. This discrepancy, about twice that for the isotropic moments, is hardly surprising because of the large measurement errors in the rotational intensities[2] and our simplification of treating the various anisotropic contributions to the line shape as one. However, theoretical and empirical slopes describing the temperature dependences (Fig. 5) roughly match thus lending credibility to the constrained fitting approach.

Although we have selected what we considered the presently best potential and induced dipole data available in Table II, results based on other potentials are given in Table III for comparison. Except for the LJ 6–12 potential, which gives much larger values because of its small root $\sigma = 2.75$ Å, the other potential and dipole models give results within roughly 15% of the theoretical values given in Table II, which we consider the best theoretical estimates.

V. RANGE PARAMETER ρ

The induced dipole functions are defined in the Appendix. The empirical range parameter ρ_i [Eq. (A3)] can be obtained from the ratio α_i/γ_i (with $C_7 = 0$) according to[5]

$$\rho^2 = \frac{kT}{m}\,\tau_{1i}\tau_{2i}\left[1 + 2\left(\frac{\rho}{\sigma}\right)^2 \frac{I_2(2\sigma/\rho)}{I_0(2\sigma/\rho)}\right]. \qquad (27)$$

The only dependence on the potential is through the integrals $I_n(\xi)$, which are defined in the Appendix [Eq. (A8)]. However, I_2 and I_0 are approximately equal, and since $(\rho/\sigma)^2 \cong 0.01$, the value of ρ is only slightly dependent on the exact value of σ and the integrals. With Eq. (15), we thus obtain the range of the exponential isotropic overlap directly as

$$\rho = 0.336 \text{ Å} . \qquad (28)$$

The accuracy in ρ amounts to about one-half of that for the product $\tau_1\tau_2$, whose statistical uncertainty is only $\sim 1\%$. However, an absolute error estimate is not feasible and may be larger than that.

If the interaction potential is accurately known, particularly at separations R from 2.0 and 3.5 Å that are most critical for collision-induced absorption, a somewhat more involved procedure which determines both the range and strength of the induced dipole is possible. We think that the empirical potential[17] is reliable at such separations and describe here briefly the results obtained by the alternative method, which resorts to solving transcendental simultaneous equations by iteration. With the relationships of the Appendix, we define two equations for the unknowns as

$$F(\mu_i, \rho_i) = 4\pi \int_0^\infty [A_i(R)]^2 g(R) R^2\, dR - S_i = 0 , \qquad (29)$$

$$G(\mu_i, \rho_i) = S_i \left\{ \frac{2\pi\hbar}{m} \int_0^\infty \left[\left(\frac{dA_i}{dR}\right)^2 + \frac{a_i}{R^2}\,[A_i(R)]^2 \right] \times g(R) R^2\, dR \right\}^{-1} - \frac{\tau_{1i}\tau_{2i}}{\tau_0} = 0 , \qquad (30)$$

TABLE IV. Empirical range and strength of induced dipole components.[a]

Isotropic component	ρ_i/Å	$\mu_i/(10^{-2}$ a.u.)[b,c]	weight
77 K	0.339	0.26	1
195 K	0.340	0.27	3
292 K	0.332	0.26	2
weighted mean	0.337 ± 1%	0.27 ± 2%	
Anisotropic component	ρ_q/Å	$\mu_q/(10^{-2}$ a.u.)[b,c]	weight
77 K	0.195	0.021	1
195 K	0.242	0.030	3
292 K	0.280	0.035	2
weighted mean	0.25 ± 8%	0.030 ± 11%	

[a]Based on the constrained fits, the Wormer-van Dijk induced dipole (Ref. 16) and the Gengenbach-Hahn potential (Ref. 17).
[b]Dipole moment at potential zero (R = 3.001 Å).
[c]1 a.u. $= ea_0 = 2.5418\times10^{-18}$ esu $= 8.4784\times10^{-30}$ $C\cdot m$.

with S_i, τ_{1i}, τ_{2i} known from Table I, and $a_i = 2$. Subscripts i can also be replaced by q, with $a_q = 12$. This set of equations can be solved by iteration if suitable starting values [for example Eq. (28)] are provided. In this procedure the dipole dispersion contribution with $C_7 = -61.8$ a.u. is included. The results are given in Table IV. The weighted averages, which emphasize the 195 K data at the expense of the 77 K values, amount to

$$\rho_i = 0.337\ \text{Å} \pm 1\%\ ;\ \mu_i = 0.0027\ \text{a.u.} \pm 2\%\ . \tag{31}$$

The range ρ_i is in agreement with Eq. (28). Errors quoted reflect the statistical part of the uncertainty (standard deviation of the mean); the absolute error could be greater. Similarly, for the anisotropic component we find

$$\rho_q = 0.25\ \text{Å} \pm 8\%\ ;\ \mu_q = 0.00030\ \text{a.u.} \pm 11\% \tag{32}$$

The isotropic range parameter, Eq. (31), can be compared with previous determinations. The *ab initio* theory indicates a value of 0.307 Å when dispersion ($C_7 = -61.8$ a.u.) is accounted for.[15] Wormer and van Dijk reinvestigated[16] the induced dipole and obtained the value of 0.323 Å. Poll and Hunt[22] presented a moment analysis of the collision-induced fundamental band and get, with a dispersion-free model, a range of 0.330 Å.

The isotropic strength parameter μ_i can be compared with the *ab initio* values of Berns *et al.*[15]: 0.0022 a.u., and of Worner and van Dijk,[16] 0.0021 a.u. These values are ≈ 20% smaller than the present experimentally determined result. However, the theoretical spectral moments, which depend on both μ_i and ρ_i, are in much better agreement with the measurement. The observed differences between theory and measurement may be related in part to inaccuracies in the data and the difficulty in obtaining an accurate decomposition of the spectrum and to inaccuracy in the theoretical induced dipole model.

We briefly state that theory[16] indicates $\rho_q = 0.433$ Å and $\mu_q = 0.0003$ a.u., which should be compared with the experimental results $\rho_q = 0.25$ Å and $\mu_q = 0.00030$ a.u.

In conclusion, we note that this work represents the first attempt at a detailed analysis of the translational-rotational band due to H_2–He collisions. In particular, we have decomposed the spectrum into the induced isotropic overlap component and anisotropic components. Analysis of the former yields induced dipole parameters in reasonable agreement with *ab initio* theory. Furthermore, progress has been made in analytically representing the H_2–He spectrum, which should be useful for applications to planetary atmospheres.

ACKNOWLEDGMENT

The work of Dr. G. Birnbaum was supported by a contract from the Jet Propulsion Laboratory, sponsored by the Planetary Atmospheres Program, NASA.

APPENDIX

The relationships between the various strength parameters, time constants, and invariants of the spectra [Eqs. (23)–(26)] can be obtained from the substitution of the spectral model Eq. (1) into Eqs. (21) and (22).[5] If instead exact moment relations are used,[24] a number of important relationships result which connect the spectral invariants with dipole components and potential functions. Specifically, the moments may be calculated as sums of an isotropic and several anisotropic dipole components, according to[14]

$$\gamma = \frac{2\pi^2}{3kTc}\sum_{L\lambda}\langle A^2_{L\lambda}(R)\rangle = \frac{2\pi^2}{3kTc}\sum_{L\lambda}4\pi\int_0^\infty [A_{L\lambda}(R)]^2 \times g(R)\,R^2\,dR\ , \tag{A1}$$

$$\alpha_1 = \frac{2\pi^2}{3c}\sum_{L\lambda}4\pi\int_0^\infty \left[\frac{1}{m}\left(\frac{dA_{L\lambda}}{dR}\right)^2 + \left(\frac{\lambda(\lambda+1)}{I} + \frac{L(L+1)}{mR^2}\right)[A_{L\lambda}(R)]^2\right] g(R)\,R^2\,dR\ . \tag{A2}$$

We note that

$$\sum_{L\lambda}[A_{L\lambda}(R)]^2 = \langle\boldsymbol{\mu}(\mathbf{R},\boldsymbol{\Omega})^2\rangle_0\ ,$$

where $\boldsymbol{\mu}(\mathbf{R},\boldsymbol{\Omega})$ is the induced dipole, $\boldsymbol{\Omega}$ is the orientation of H_2 and $\langle\cdots\rangle_0$ denotes an unweighted average over $\boldsymbol{\Omega}$ and the unit vector $\mathbf{R}$. Here, m is the reduced mass and $g(R)$ designates the low-density limit of the pair distribution function of an isotropic interaction potential. Quantum mechanical corrections to the classical expression,

$$g(R) = \exp[-V_0(R)/kT]\ ,$$

are necessary for the He–H_2 system at all temperatures considered.

The sum over the induced-dipole expansion coefficients $A_{L\lambda}(R)$ contain only three significant terms, namely $L, \lambda = 1, 0$; 1, 2 and 3, 2. These exponential coefficients have units of dipole moment. The isotropic expansion coefficient can be approximated by

$$A_{10}(R) = \mu_{10}\exp[-(R-\sigma)/\rho_{10}] + C_7/R^7\ , \tag{A3}$$

where the first term is due to the electron overlap interaction and the second, longer range term is a dispersion contribution. The anisotropic expansion coefficients are modeled by[14]

$$A_{12}(R) = \mu_{12}\exp[-(R-\sigma)/\rho_{12}]\ , \tag{A4}$$

$$A_{32}(R) = \mu_{32} \exp[-(R-\sigma)/\rho_{32}] + \sqrt{3}\,\alpha\theta/R^4 , \tag{A5}$$

where μ_{12} and μ_{32} are amplitudes of the exponential short-range overlap contributions. The second term in Eq. (A5) is the quadrupole-induced dipole contribution where α designates the helium polarizability and θ the H_2 quadrupole moment. As mentioned previously, recent *ab initio* calculations give a more complex form for the exponential[25] and $A_{12}(R)$ is much smaller than $A_{32}(R)$.

The invariants γ_{1i} and α_{1i} ($L=1$, $\lambda=0$) can be written as

$$\gamma_{1i} = \frac{2\pi^2\beta\sigma^3}{3c}\left[\mu_i^2 I_0(2\sigma/\rho_i) + \mu_i C_7\sigma^7 I_7(\sigma/\rho_i) + C_7^2\sigma^{14} I_{14}(0)\right] , \tag{A6}$$

$$\alpha_{1i} = \frac{2\pi^2\sigma}{3cm}\left[\left(\frac{\sigma}{\rho_i}\right)^2 \mu_i^2 I_0(2\sigma/\rho_i) + 14\left(\frac{\sigma}{\rho_i}\right)\sigma^9 C_7 I_8(\sigma/\rho_i) + 49\,\sigma^{18} C_7^2 I_{16}(0) + \frac{3c}{\pi\beta\sigma^2}\gamma_{1i}\right] , \tag{A7}$$

where the term containing γ_{1i} in Eq. (A7), the angular contribution, is negligible compared with all the other terms, the radial contribution. The anisotropic contributions γ_{1q} and α_{1q} plus the very small hexadecapole contribution are given respectively by Eqs. (A9) and (A11) of Ref. 3 with κ, the anisotropic polarizability factor, set equal to zero, since the polarizability of He is spherical, and with γ_1 divided by 2 because there is only the dipole induced in He by H_2.

The I integrals used in Eqs. (A6) and (A7) are defined as

$$I_n(\xi) = 4\pi \int_0^\infty g(x)\, x^{-n} \exp[-(x-1)\xi]\, x^2\, dx . \tag{A8}$$

The low-density limit of the pair distribution function is written $g(x)$, with $x = R/\sigma$. Since the anisotropy of the H_2–He potential is minor, an isotropic potential is commonly assumed.

[1] L. M. Trafton and G. Munch, J. Atm. Sci. 26, 813 (1969); G. S. Orton and A. P. Ingersoll, in *Jupiter*, edited by I. Gehrels (University of Arizona, Tucson, 1976), p. 207; and D. Gautier, B. Conrath, M. Flasar, R. Hanel, V. Kunde, A. Chedin, and N. Scott, J. Geophys. Res. 86, 8713 (1981).

[2] G. Birnbaum, J. Quant. Spectrosc. Radiat. Transfer 19, 51 (1978).

[3] G. Bachet, G. Birnbaum, E. R. Cohen, and P. Dore, Can. J. Phys. (to be published).

[4] P. Dore, L. Nencini, and G. Birnbaum, J. Quant. Spectrosc. Radiat. Transfer. (to be published).

[5] G. Birnbaum and E. R. Cohen, J. Can. Phys. 54, 593 (1976).

[6] E. R. Cohen and G. Birnbaum, National Bureau of Standards Report NBSIR 80-2175(R), April 1981. Note that inadvertantly the H_2–He moments were given incorrectly. These should read at 77, 195 and 292 K, respectively, in the same units; Table 4—$\gamma_{1i} = 0.977$; 0.915; 0.894; $\gamma_{1q} = 0.816$; 0.792; 0.828; and Table 6—$\alpha_{1i} = 0.576$; 1.09; 1.86; $\alpha_{1q} = 0.403$; 0.971; 1.511.

[7] B. P. Stoicheff, Can. J. Phys. 35, 730 (1957).

[8] J. D. Poll, J. L. Hunt, and J. W. MacTaggart, Can. J. Phys. 53, 954 (1975).

[9] J. W. MacTaggart and H. L. Welsh, Can. J. Phys. 51, 158 (1973).

[10] *Handbook of Mathematical Functions*, edited by M. Abramowitz and I. A. Stegun, National Bureau of Standards, Appl. Math. Series 55 (1964).

[11] J. J. More, in *Numerical Analysis*, edited by G. A. Watson (Springer, New York, 1977). We use the Fortran program written by K. L. Hiebert, SLA (1980).

[12] J. van Kranendonk, *Intermolecular Spectroscopy and Dynamical Properties of Dense Systems*, E. Fermi, International School of Physics, Italian Physics Society (North-Holland, Amsterdam, 1980), Vol. LXXV, p. 77.

[13] S. Cunsolo and H. P. Welsh, Can. J. Phys. 50, 2958 (1972).

[14] J. D. Poll and J. van Kranendonk, Can. J. Phys. 39, 189 (1961).

[15] R. M. Berns, P. E. S. Wormer, F. Mulder, and A. van der Avoird, J. Chem. Phys. 69, 2102 (1978).

[16] P. E. S. Wormer and G. van Dijk, J. Chem. Phys. 70, 5695 (1979).

[17] R. Gengenbach and C. Hahn, Chem. Phys. Lett. 15, 604 (1972).

[18] W. Meyer, P. C. Hariharan, and W. Kutzelnigg, J. Chem. Phys. 73, 1880 (1980).

[19] F. Mulder, A. van der Avoird, and P. E. S. Wormer, Mol. Phys. 37, 159 (1979).

[20] A. R. W. McKellar, J. W. MacTaggert, and H. L. Welsh, Can. J. Phys. 53, 2026 (1975).

[21] R. W. Hartye, C. G. Gray, J. D. Poll, and M. S. Miller, Can. J. Phys. 29, 825 (1975).

[22] J. D. Poll and J. L. Hunt, Can. J. Phys. 54, 461 (1976).

[23] P. Gibbs, J. L. Hunt, and J. D. Poll, Can. J. Phys. 57, 981 (1979).

[24] G. Birnbaum, M. S. Brown, and L. Frommhold, Can. J. Phys. 59, 1544 (1981).

[25] W. Meyer (private communication).

[26] This is presumably reflected by the fact that the inverted Jacobian (the invariance matrix) of the least-mean squares fit shows less cross correlation and smaller diagonal elements at 195 K.